Global warming acceleration in satellite observed lower-tropospheric temperature

Cheng-Zhi Zou

chengzhizou60@gmail.com

George Mason University https://orcid.org/0000-0003-4124-6448

Xianjun Hao

George Mason University

John J. Qu

George Mason University

Satya Kalluri

NOAA/NESDIS Office of Low Earth Orbit Observations

Research Article

Keywords: global warming acceleration, satellite observation, temperature of lower-troposphere, ENSO and aerosol effects on global warming

Posted Date: April 2nd, 2026

DOI: https://doi.org/10.21203/rs.3.rs-9283491/v1

Additional Declarations: The authors declare no competing interests.

Abstract

We analyze accelerated global warming over 1981–2025 using satellite-derived lower-tropospheric temperature (TLT) data and examine its relationship to the pronounced warming observed during 2023–2024. To reduce uncertainty and improve the robustness of acceleration detection, an adjusted TLT record is constructed by removing ENSO- and aerosol-related variability. This adjustment reduces the magnitude of TLT annual variability by nearly 50%, which greatly increases the robustness and reliability of acceleration detection. We therefore recommend using the ENSO–aerosol-adjusted TLT for long-term trend and acceleration analyses. With the adjusted TLT, statistically significant warming trends of up to 0.482 ± 0.113°C decade^{-1} are found from 2015 onward across all satellite and reanalysis datasets examined in this study, representing an increase of approximately four to five times relative to the pre-2015 period. This large trend, however, is only a conservative estimate. At the upper end, statistically significant acceleration rates of up to 0.48 ± 0.12°C decade^{-2} are inferred near 2024, indicating that the recent temperature jumps are part of an ongoing acceleration amplified by the El Niño event. Projections based on the accelerated trend estimates suggest the potential for an additional 0.5–1.0°C of warming within the next decade.

Introduction

The years 2023–2024 have recorded the highest global temperatures ever observed on Earth, due to the combined effects of human-induced global warming and an El Niño event[1-4]. This warming surpassed previous records by 0.2°–0.4°C during the latter half of 2023 and the first half of 2024—an unprecedented margin on a global scale[1]. Such exceptional warming exceeds expectations from climate model simulations, prompting renewed investigations into both short-term climate forcing anomalies and long-term trends[1-2]. A recent study suggests that the near-surface temperature jump during 2023–2024 is associated with a decrease in low cloud cover, leading to reduced planetary albedo and increased absorption of solar radiation[5].

However, it remains unclear whether this temperature jump is part of an accelerated long-term warming trend. Several studies have examined acceleration in global mean surface temperature (GMST) records. One such study reported an acceleration rate of 0.049°C per decade[2] across multiple surface temperature datasets for the period 1980–2020(ref. 6), although confidence in these estimates was low. Another recent study using GMST data found no statistically significant changes in the warming rate during 1970–2024, despite the record-breaking temperatures observed in 2023 (ref. 7). However, when natural variability caused by exogenous factors—including the El Niño–Southern Oscillation (ENSO), volcanism, and the solar cycle—was removed from the GMST, accelerations were found to be statistically significant (ref. 8).

Warming acceleration is a fundamental metric that influences both long-term, multi-decadal climate trends and short-term, year-to-year temperature spikes. It represents a subtle signal superimposed on the long-term temperature trend, which is itself relatively small compared to the annual and seasonal

variability in climate data. Determining acceleration with high confidence faces two key challenges. First, it is essential to ensure the statistical significance of any detected acceleration in a time series to assess its reliability. This generally requires the time series to be sufficiently long. Second, accurately identifying warming acceleration requires high-quality climate data records (CDRs). Unfortunately, methodologies used for bias correction in CDR construction can influence estimates of both warming slowdowns and accelerations[9-10]. Examining reliable and as many CDRs as possible to determine a statistically significant acceleration rate is essential.

Spaceborne, Earth-orbiting satellites provide near-surface global temperature measurements that complement GMST studies. The temperature record from satellite microwave sounder observations spans 46 years, from 1979 to the present[10-12]. These data have been extensively used in climate change research over the past three decades[13-23]. With 46 years of satellite data now available, investigating global warming acceleration has become more feasible and robust. Advances in satellite data processing and a deeper understanding of data homogenization issues[10] further support such studies. Moreover, the availability of multiple satellite datasets, each processed using different homogenization algorithms, provide a measure of structural uncertainty.

In this study, we employ multiple satellite temperature of lower-troposphere (TLT) datasets and analytical methods to investigate warming acceleration over the past 45 years. We identify statistically significant acceleration rates beginning around 2000 and large trend changes near 2015. The strength of this acceleration signal supports the conclusion that the 2023–2024 temperature jump is part of an ongoing acceleration process. Given the statistical significance of the detected acceleration, we develop simple models to project global TLT warming over the next decade.

The satellite TLT data record

We use lower-tropospheric temperature (TLT) products from three groups—NOAA (ref. 10), the University of Alabama at Huntsville (UAH, ref. 11), and Remote Sensing Systems (RSS, ref 12)—to investigate global warming acceleration. TLT measures a weighted average temperature from the surface to ~12 km, with peak sensitivity near 2.5 km, and is derived from microwave sounder observations onboard multiple polar-orbiting satellites since 1981 (see Methods section). TLT trends have been widely compared with GMST in previous studies[13].

We also analyze ERA5 reanalysis output(ref. 24). An equivalent TLT is constructed from ERA5 temperature profiles using the TLT weighting function (Extended Data Fig. 1). Because microwave sounder observations are assimilated into ERA5, the ERA5-derived TLT provides a complementary perspective and physically consistent forcing fields linked to TLT variability.

Figure 1a shows global annual-mean TLT anomalies for 1981–2025. The 2023–2024 jumps are clearly evident, marking the highest values on record across all datasets. Linear trends over 1981–2025

are 0.152, 0.162, 0.241, and 0.199 °C decade⁻¹ for NOAA, UAH, RSS, and ERA5, respectively, reflecting structural uncertainty among the datasets.

Figure 1b shows time series of differences between datasets. These differences largely arise from calibration treatments. Relative to NOAA, RSS shows a pronounced warming drift during 1990–2004, associated with known spurious MSU channel-2 drifts from NOAA-11 through NOAA-14[10, 25-26] that are corrected in NOAA[10] and mitigated in UAH[11] but not explicitly removed in RSS. After 2000, UAH exhibits a relative cooling drift linked to biases in NOAA-15 AMSU-A channel 5, which are corrected in NOAA[10] but retained in UAH.

The ERA5 TLT shows an upward drift relative to NOAA after about 2000 while exhibiting similar trends prior to 2000. This divergence likely reflects differing bias treatments in reanalysis assimilation versus direct satellite merging. In ERA-Interim, a cooling drift in Aqua AMSU-A mid-tropospheric channels was identified and removed during data assimilation[25]. In contrast, independent comparisons show highly consistent trends between Aqua AMSU-A and Suomi National Polar-orbiting Partnership (SNPP) ATMS observations due to their stable sun-synchronous orbits[19]. The NOAA TLT dataset uses Aqua AMSU-A and SNPP ATMS as reference sensors and does not apply bias-drift corrections prior to merging[10,20].

These differences in calibration and satellite bias handling affect not only long-term linear trends but also the identification of acceleration signals, as demonstrated below.

Fitting Models to the Global Mean TLT Time Series

We aim to identify whether warming in the global mean TLT is accelerating. Instantaneous acceleration rate can be calculated as the second derivative of the TLT time series, but annual variability adds substantial noise, making this measure unreliable. For this reason, acceleration is usually estimated using a fitted model, whose reliability depends on its statistical significance.

Annual variability strongly affects statistical significance. Two major contributors to this variability are the El Niño–Southern Oscillation[27-29] and changes in sulfate aerosols, which scatter and reflect incoming solar radiation[30-31]. To reduce their influence, we created an adjusted TLT record in which ENSO and aerosol effects are removed. Similar approaches have been used in previous studies[8,32-33]. ENSO is accounted for using the NINO 3.4 index[29-34] with a 5-month lag (Extended Data Figs. 3 and 4), and aerosols are represented using the MERRA-2 reanalysis[35] (Extended Data Fig. 3), with an 8-month lag (Extended Data Fig. 4). The MERRA-2 aerosols include tropospheric sulfate from fossil fuel combustion and stratospheric aerosols from volcanic eruptions. The resulting product is referred to as the ENSO-aerosol-adjusted TLT (Extended Data Fig. 2).

We examined two types of fitting models. Note that the fitting model uses data from 1981–2024, with 2025 reserved as a test of the model projection in the climate projection section. The first is a

piecewise linear regression model, which has been widely used to study changes in GMST trends[7-8,36]. This method divides a time series into segments, with major trend shifts occurring at "changepoints." A changepoint near 2012 in GMST over the period 1970–2023 was identified by ref. 7, although the associated trend change was not statistically significant. After removing aerosol and ENSO effects, a statistically significant changepoint near 2015 was identified in ref. 8. Using the same approach, we identified statistically significant trend changepoints near 2015 in the ENSO-aerosol-adjusted TLT for all datasets (Extended Data Fig. 5), consistent with the GMST behavior reported in ref. 8. For the original TLT, changepoints were identified near 2013 (Extended Data Fi. 5). Their timing aligns with the GMST behavior reported in ref. 7, but the trend changes are statistically significant only for NOAA and ERA5, not for UAH and RSS (Extended Data Fig. 5). The statistical significance observed across all datasets in the ENSO–aerosol-adjusted time series arises from the substantial reduction in variability, which is only about 50% of that in the original TLT (discussion in Methods section). This variability reduction markedly increases the robustness of the detected acceleration signals. As a result, our discussion focuses on the ENSO–aerosol-adjusted time series in the following.

Second, we examined polynomial fits from linear to fifth order for all datasets (Extended Data Fig. 6). NOAA and ERA5 show consistent behavior between the original and ENSO-aerosol-adjusted TLT series. The fourth- and fifth-order curves closely resemble the cubic fit, which exhibits a wave-like structure with inflection points near 2000 for NOAA and 1997 for ERA5, in contrast to the linear and quadratic fits that lack inflection points. RMSE decreases from the linear model and levels off at the cubic fit (Extended Data Fig. 7), indicating that third- or higher-order polynomials adequately capture the data structure. However, only the linear through cubic fits are statistically significant ($p < 0.05$), while the fourth- and fifth-order fits are not (Extended Data Fig. 7). Taken together, these results indicate that the cubic polynomial is the most appropriate model for both the original and ENSO-aerosol-adjusted NOAA and ERA5 time series.

UAH and RSS exhibit different behavior between the original and ENSO-aerosol-adjusted TLT time series. For the original UAH and RSS datasets, only the linear fits are statistically significant, whereas for the adjusted datasets, statistically significant fits extend up to the fourth-order models (Extended Data Fig. 7). This suggests that differences in calibration and satellite-bias handling influence the statistical significance of TLT fitting models across datasets; nevertheless, the ENSO-aerosol-adjusted TLT consistently yields statistically significant cubic fits for all datasets. We note that the cubic fits closely resemble the locally weighted regression(LOESS) smoothing[37-38] (Extended Data Fig. 8). Thus, the cubic fit may be interpretated as an explicit representation of the LOESS smooth.

Figures 2a shows the piecewise and cubic fits for the adjusted TLT time series and Figure 2b shows their residuals. The residuals are dominated by 3–4-year variability with zero trends. This variability likely reflects internal climate variability, dominated by residual ENSO effects[32-33], with possible contributions from Quasi-Biennial Oscillation (QBO)-related aliasing through stratosphere–troposphere coupling[39-40]. The magnitude of this variability is quite small, in the range of 0.061–0.077 °C. The variability is similar for the piecewise and cubic models, suggesting that they provide comparably

strong fits. Figure 3 shows similar plot but for the original time series. Trend uncertainty in the adjusted time series is approximately half that of the original series because of its substantially reduced variability, resulting in high confidence in the fits to the ENSO–aerosol-adjusted TLT.

Although both fits are statistically significant, the piecewise and cubic models exhibit distinctly different acceleration behavior. The piecewise models produce trend jumps at the changepoints, with much larger trends after the changepoints. Actual trends increase from 0.080 to 0.503 °C decade^{-1} for NOAA and from 0.103 to 0.423 °C decade^{-1} for UAH from before to after 2015, representing approximately four- to five-fold increases in magnitude. For RSS and ERA5, the ratios of trend change are slightly smaller due to relatively larger pre-2015 trends; however, their post-2015 trends also fall in the range of 0.463–0.539 °C decade^{-1} (Figure 2a). On average, the post-2015 trends are 0.482 ± 0.113 °C decade^{-1} across all four datasets examined here. Despite the large trend jumps, the instantaneous acceleration rate, defined as the second derivative of the time series, is nonzero only at the changepoints (singular points) and remains zero elsewhere in the piecewise fits.

In contrast, the cubic model exhibits a continuous linear increase in acceleration (Figure 4). The acceleration evolves from negative to positive values, crossing zero around 2000 for NOAA and UAH and around 1997 for RSS and ERA5. This timing represents the onset of acceleration. By 2024, the acceleration in the adjusted TLT reaches 0.579, 0.410, and 0.456 °C decade^{-2} for NOAA, UAH, and ERA5, respectively (Figure 4), with a mean of 0.482 ± 0.123 °C decade^{-2}. This is nearly an order of magnitude larger than acceleration estimates derived from GMST datasets using quadratic fits(ref. 6). The RSS dataset shows smaller acceleration (0.238 °C decade^{-2}), likely because it does not correct the spurious warming associated with NOAA-11 to NOAA-14 satellites, leading to larger early-period trends (Figure 1) and consequently smaller inferred accelerations; it is therefore not included in the mean reported here.

Two common features emerge across all datasets. (1) The linear trends over 1981–2024 for the ENSO–aerosol-adjusted TLT are smaller than those of the original TLT by about 0.016–0.020 °C decade^{-1} for all datasets (Figures 2 and 3). In addition, the total changes (maximum at 2024 minus minimum at 1981) in the adjusted TLT are reduced by about 0.032–0.069 °C relative to the original TLT for both fitting models. These differences reflect the net cooling effect of aerosols on the climate system. (2) The temperature jumps during 2023–2024 can be largely attributed to the accelerated warming captured by the fitted models. For example, in the NOAA adjusted time series, the linear trend of 0.130 °C decade^{-1} would yield only 0.117 °C of warming over the 9-year period from 2015 to 2024. When acceleration is included, the piecewise fit produces 0.452 °C of warming during the same period, an increase of 0.335 °C. Other datasets show comparable additional warming due to acceleration, ranging from 0.220 °C for RSS to 0.324 °C for ERA5. The cubic fits yield similar additional warming during 2015–2024 compared to linear warming. The remaining warming in observations is attributable to El Niño effects, estimated as the residuals between observations and the accelerated-warming fits during 2023–2024 (Figure 3b), with magnitudes of approximately 0.2–0.3 °C depending on the dataset and fitting approach. The acceleration-driven warming suggests that the 2023–2024 temperature jumps are part of an ongoing acceleration.

Projection of future climate change

A significant implication of the detected acceleration is its potential impact on future warming. Because both the cubic and piecewise fitting models are statistically significant for all adjusted datasets, they can be used to explore projections of future climate change. Here, we use the NOAA dataset as an illustrative example. Note that statistical significance of the fits does not imply skillful projections; substantial changes in climate forcing could lead to future climate trajectories that differ from these projections. Nevertheless, it is informative to examine the projected behavior given the large acceleration rates observed during 2023–2024.

Figure 5a shows cubic and piecewise projections extending up to ten years for the ENSO–aerosol-adjusted TLT. The observed 2025 value provides an independent test of the projections. The piecewise projection closely matches the observation, with a bias of only -0.001 °C, whereas the cubic projection shows a slightly larger bias of 0.045 °C. Figure 4b presents the corresponding projections for the original TLT, but only through 2025, as projection uncertainties increase rapidly over time due to ENSO-related variability, limiting the interpretive value of longer lead times. For 2025, the projection biases for the original TLT are 0.028°C and 0.109 °C for the piecewise and cubic models, respectively—slightly larger than those for the ENSO–aerosol-adjusted series, consistent with greater ENSO-driven variability and reduced predictability. Nevertheless, both cubic and piecewise projections remain within their respective 95% confidence intervals for both the original and adjusted TLT.

Over the 10-year period (2025–2034), the piecewise model projects additional warming of 0.503 ± 0.180 °C in the adjusted TLT time series, corresponding to a warming rate approximately three times the 1981–2024 average. The cubic model projects additional warming of 1.042 ± 0.292 °C, corresponding to a warming rate five to six times the 1981–2024 average. Statistical significance warrants serious consideration of both model projections. However, because the projected climate changes differ substantially, additional information on future climate forcing is needed to assess which projection is more likely to be realized. In the absence of such information, the piecewise projection may be viewed as a conservative estimate, whereas the cubic projection represents an upper-end scenario.

Discussion

After removing ENSO and aerosol effects, robust and statistically significant post-2015 warming trends of up to 0.482 ± 0.113°C decade^{-1} are identified across all satellite and reanalysis TLT datasets. Although substantial, this represents a conservative estimate. As an upper-end scenario, statistically significant acceleration emerges around 2000 and reaches ~ 0.4–0.5°C decade^{-2} by 2024. These trends indicate that the 2023–2024 temperature jumps are part of an ongoing acceleration, amplified by El Niño, and imply an additional 0.5–1.0°C of warming over the next decade—roughly three to five times the 1981–2024 linear trend.

Despite the robustness of the detected acceleration, its physical drivers remain uncertain. While increasing well-mixed greenhouse gases, including CO_2, CH_4, and N_2O, are the dominant cause of long-

term warming[41–42], their combined radiative forcing has increased approximately linearly over 1981–2024 (Extended Data Fig. 9), making it difficult to attribute the pronounced recent acceleration to greenhouse forcing alone. Reduced sulfate aerosol cooling following International Maritime Organization regulations[43] has also been proposed as a contributor to recent accelerated warming[44–45]. However, because aerosol effects are largely removed in the adjusted TLT series, the persistence of strong acceleration suggests that aerosols are unlikely to be the primary driver.

Declining planetary albedo[46–47] and associated cloud changes have been implicated in recent surface warming[5], but cloud processes remain a major source of uncertainty[48–49], and current observations are insufficient to quantify their contribution to TLT acceleration. Similarly, increased atmospheric moisture provides positive feedback to temperature changes. Strong TLT–moisture coupling has been identified over tropical oceans, where the ratio of column water vapor trends to atmospheric temperature remains relatively stable in coupled ocean–atmosphere model simulations[50–52]. However, observed moisture–temperature relationships differ from model expectations[50,53], limiting their explanatory power.

Given these unresolved mechanisms, the projections presented here are necessarily data-driven. Although physically based coupled models are widely used for climate projections[42,44,52], they have not consistently reproduced satellite-observed atmospheric trends[23,52] or the magnitude of the 2023–2024 temperature increases[1]. Data-driven approaches therefore provide a complementary perspective for near-term projections. Nevertheless, given the pronounced late-record acceleration, these projections should be interpreted cautiously, as unforeseen changes in forcing or climate events could alter future trajectories.

Online content

Methods, additional references, Nature Portfolio reporting summaries, source data, extended data, supplementary information, acknowledgements, peer review information, details of author contributions and competing interests, and statements of data and code availability are provided below and will be available online upon acceptance of the manuscript.

Declarations

Competing interests

The authors declare no competing interests

Author contributions

C.-Z.Z. conceived the study and drafted the manuscript. X.H. implemented the methodology for all calculations and figure preparation. J.J.Q. and S.K. contributed to editing and revising the manuscript.

Acknowledgement

The work was supported by the NOAA/Office of Low Earth Orbit Observations (LEO) Proving Ground and Risk Reduction (PGRR) Program, NOAA/National Centers for Environmental Information (NCEI) Climate Data Record (CDR) Program, and NSF 17–516 Industry-University Cooperative Research Centers Program (Award Number 1841520).

Data Availability

All data used in this study are publicly available and are listed below:

NOAA V5.0 TLT dataset: http://wamis.gmu.edu/cdr/products.html

UAH v6.1 TLT dataset: https://www.nsstc.uah.edu/data/msu/v6.1/tlt/

RSS V4.0 TLT dataset: https://data.remss.com/msu/data/netcdf/

ERA5 dataset: https://cds.climate.copernicus.eu/datasets/reanalysis-era5-single-levels-monthly-means?tab=download

All data generated to evaluate the conclusions of this paper are included in the manuscript and are available at http://wamis.gmu.edu/cdr/products.html.

Code availability

Codes used to create the figures are available at http://wamis.gmu.edu/cdr/pub/code_paper/index.html.

References

1. Schmidt G (2024) Climate models can't explain 2023's huge heat anomaly — we could be in uncharted territory. Nature 627:467
2. Po-Chedley S, Christy JR, Haimberger L, Mears CA, Zou C-Z (2024) Tropospheric temperature. In *State of the Climate in 2023*. Bull Am Meteorol Soc 105:S39–S41
3. Copernicus (2024) is the first year to exceed 1.5°C above pre-industrial level (2025); available at https://climate.copernicus.eu/copernicus-2024-first-year-exceed-15degc-above-pre-industrial-level
4. NOAA National Centers for Environmental Information. Annual 2024 Global Climate Report (2025) ; available at https://www.ncei.noaa.gov/access/monitoring/monthly-report/global/202413
5. Groessling HF, Rackow T, Jung T (2025) Recent global temperature surge intensified by record-low planetary albedo. Science 387:68–73
6. Richardson MT (2022) Prospects for detecting accelerated global warming. *Geophys. Res. Lett.* 49, e2021GL095782

7. Beaulieu C, Gallagher C, Killick R, Lund R, Shi X (2024) A recent surge in global warming is not detectable yet. Commun Earth Environ 5:576
8. Rahmstorf S, Foster G (2025) Global warming has accelerated significantly. *Research Square* preprint
9. Karl TR et al (2015) Possible artifacts of data biases in the recent global surface warming hiatus. Science 348:1469–1472
10. Zou C-Z, Xu H, Hao X, Liu Q (2022) Mid-tropospheric layer temperature record derived from satellite microwave sounder observations with backward merging approach. *J. Geophys. Res. Atmos.* 128, eJD037472 (2023)
11. Spencer RW, Christy JR, Braswell WD (2017) UAH version 6 global satellite temperature products: methodology and results. Asia-Pac J Atmos Sci 53:121–130
12. Mears C, Wentz FJ (2017) A satellite-derived lower-tropospheric atmospheric temperature dataset using an optimized adjustment for diurnal effects. J Clim 30:7695–7718
13. Spencer RW, Christy JR (1992) Precision and radiosonde validation of satellite gridpoint temperature anomalies. Part II: tropospheric retrieval and trends during 1979–90. J Clim 5:858–866
14. Christy JR, Spencer RW, Norris WB, Braswell WD (2003) Error estimates of version 5.0 of MSU–AMSU bulk atmospheric temperature. J Atmos Ocean Technol 20:613–629
15. Mears CA, Schabel MC, Wentz FJ (2003) A reanalysis of the MSU channel 2 tropospheric temperature record. J Clim 16:3650–3664
16. Mears CA, Wentz FJ, Thorne P, Bernie D (2011) Assessing uncertainty in estimates of atmospheric temperature changes from MSU and AMSU using a Monte-Carlo estimation technique. J Geophys Res 116:D08112
17. Fu Q, Johanson CM, Wallace JM, Reichler T (2006) Enhanced mid-latitude tropospheric warming in satellite measurements. Science 312:1179
18. Fu Q, Johanson CM, Warren SG, Seidel DJ (2004) Contribution of stratospheric cooling to satellite-inferred tropospheric trends. Nature 429:55–58
19. Zou C-Z, Goldberg M, Hao X (2018) New generation of U.S. satellite microwave sounder achieves high radiometric stability performance for reliable climate change detection. Sci Adv 4:eaau0049
20. Zou C-Z, Xu H, Hao X, Fu Q (2021) Post-millennium atmospheric temperature trends observed by satellites on stable orbits. *Geophys. Res. Lett.* 48, e2021GL093291
21. Santer BD et al (2017) Causes of differences in model and satellite tropospheric warming rates. Nat Geosci 10:478–485
22. Steiner AK et al (2020) Observed temperature changes in the troposphere and stratosphere from 1979 to 2018. J Clim 33:1865–1884
23. McKitrick R, Christy JR (2020) Pervasive warming bias in CMIP6 tropospheric layers. Earth Space Sci 7:e2020EA001281
24. Hersbach H et al (2020) The ERA5 global reanalysis. Q J R Meteorol Soc 146:1999–2049

25. Dee DP, Uppala S (2009) Variational bias correction of satellite radiance data in the ERA-Interim reanalysis. Q J R Meteorol Soc 135:1830–1841
26. Christy JR et al (2018) Examination of space-based bulk atmospheric temperatures used in climate research. Int J Remote Sens 39:3580–3607
27. Bjerknes J (1969) Atmospheric teleconnections from the equatorial Pacific. Mon Weather Rev 97:163–172
28. Trenberth KE et al (2002) Evolution of El Niño–Southern Oscillation and global atmospheric surface temperatures. J Geophys Res 107:4065
29. Wolter K, Timlin MS (2011) El Niño/Southern Oscillation behaviour since 1871 as diagnosed in an extended multivariate ENSO index (MEI.ext). Int J Climatol 31:1074–1087
30. Charlson RJ et al (1992) Climate forcing by anthropogenic aerosols. Science 255:423–430
31. Li J et al (2022) Scattering and absorbing aerosols in the climate system. Nat Rev Earth Environ 3:363–379
32. Santer BD et al (2001) Accounting for the effects of volcanoes and ENSO in comparisons of modeled and observed temperature trends. J Geophys Res 106:28033–28059
33. Foster G, Rahmstorf S (2011) Global temperature evolution 1979–2010. Environ Res Lett 6:044022
34. Feng M et al (2021) Niño 4 west (Niño-4W) sea surface temperature variability. J Geophys Res Oceans 126:e2021JC017591
35. Randles CA et al (2017) The MERRA-2 aerosol reanalysis, 1980 onward. Part I: system description and data assimilation evaluation. J Clim 30:6823–6850
36. Cahill N, Rahmstorf S, Parnell AC (2015) Changepoints of global temperature. Environ Res Lett 10:084002
37. Cleveland WS (1979) Robust locally weighted regression and smoothing scatterplots. J Am Stat Assoc 74:829–836
38. Cleveland WS, Devlin SJ (1988) Locally weighted regression: an approach to regression analysis by local fitting. J Am Stat Assoc 83:596–610
39. Baldwin MP et al (2001) The quasi-biennial oscillation. Rev Geophys 39:179–229
40. Garfinkel CI, Hartmann DL (2011) The influence of the quasi-biennial oscillation on the troposphere in winter in a hierarchy of models. J Atmos Sci 68:1273–1289
41. Manabe S, Wetherald RT (1967) Thermal equilibrium of the atmosphere with a given distribution of relative humidity. J Atmos Sci 24:241–259
42. IPCC (2014) Climate Change 2014: Synthesis Report. IPCC
43. International Maritime Organization. IMO 2020 – cutting sulphur oxide emissions (2026) ; available at https://www.imo.org/en/MediaCentre/HotTopics/Pages/Sulphur-2020.aspx
44. Hansen JE et al (2023) Global warming in the pipeline. Oxf Open Clim Change 3:kgad008
45. Hansen JE et al (2025) Global warming has accelerated: are the United Nations and the public well-informed? Environ Sci Policy Sustain Dev 67:6–44

46. Loeb NG et al (2018) CERES EBAF TOA Edition-4.0 data product. J Clim 31:895–918
47. Loeb NG et al (2024) Observational assessment of changes in Earth's energy imbalance since 2000. Surv Geophys 45:1757–1783
48. Qu X, Hall A, Klein SA, Caldwell PM (2014) On the spread of changes in marine low cloud cover in climate model simulations of the 21st century. Clim Dyn 42:2603–2626
49. Bony S et al (2015) Clouds, circulation and climate sensitivity. Nat Geosci 8:261–268
50. Mears CA et al (2007) The relationship between temperature and precipitable water changes over tropical oceans. Geophys Res Lett 34:L24709
51. O'Gorman PA, Muller CJ (2010) How closely do changes in surface and column water vapour follow Clausius–Clapeyron scaling in climate change simulations? Environ Res Lett 5:025207
52. Santer BD et al (2021) Using climate model simulations to constrain observations. J Clim 34:6281–6301
53. Fu Y et al (2025) A climate data record of atmospheric moisture and sea surface temperature from satellite observations. Earth Syst Sci Data 17:4651–4670

Methods

Satellite temperature of lower-troposphere (TLT)

Three groups, including the NOAA Center for Satellite Applications and Research (NOAA, ref. 10,19-20, 54), the University of Alabama at Huntsville (UAH, ref. 11,13-14), and Remote Sensing Systems (RSS, ref. 12,15, 55-56), have developed temperature time series using satellite microwave sounder observations for layers of the lower troposphere (TLT), mid-troposphere (TMT), upper troposphere (TUT), and lower stratosphere (TLS). The weighting functions for TLT, TMT, TUT, and TLS peak roughly at 2.5, 5, 10, and 17 km above the Earth's surface, respectively. The TMT, TUT, and TLS time series are based on near-nadir observations from the Microwave Sounding Unit (MSU) channels 2, 3, and 4, with central spectral frequencies at 53.74, 54.96, and 57.95 GHz, respectively, merged with their Advanced Microwave Sounding Unit-A (AMSU-A) companion channels. The NOAA dataset also includes observations from the Advanced Technology Microwave Sounder (ATMS) onboard the SNPP (Suomi National Polar-orbiting Partnership) and NOAA-20 satellites since 2012.

This study uses TLT data. The construction algorithms for TLT differ among the three groups. The TLT data from NOAA and UAH are based on combinations of TMT, TUT, and TLS, using slightly different sets of combination coefficients (ref. 10-11, 57). In contrast, RSS's TLT is derived from combinations of different off-nadir observations of MSU channel 2 and AMSU-A channel 5 (ref. 12-13). These differing construction algorithms result in slight variations in the weighting functions among the datasets. However, the impact of the TLT weighting function differences on trends is only about 0.01 K/decade[2] (ref. 2) Consequently, these differences in TLT weighting functions would not affect the results of our analysis.

This study uses the most recent dataset versions from the three groups: NOAA V5.0, UAH V6.1, and RSS V4.0. All three groups utilized MSU observations onboard nine NOAA satellites, including TIROS-N and NOAA-6 through NOAA-14, but employed different subsets of AMSU-A and ATMS satellites. Inter-satellite calibration, quality control, and diurnal drift adjustments were performed by these groups during the satellite merging processes to remove relevant biases in the datasets. An important difference in inter-satellite calibration among these datasets is discussed in the main text.

All three satellite datasets are in the form of monthly means on 2.5° × 2.5° latitude/longitude grids. Near-global averages of TLT were calculated over areas of common coverage in the NOAA, RSS, and UAH datasets (82.5°N to 82.5°S). At the time this analysis was performed, TLT data from all the three groups for our analysis period, spanning January 1981 to December 2025, were available.

Equivalent TLT from ERA5

Equivalent TLT can be derived from climate reanalyses using atmospheric temperatures defined at specific pressure levels. Climate reanalyses combine satellite observations, atmospheric models, and meteorological data, providing a comprehensive depiction of global atmospheric temperature variability over time. Here, we use ERA5 (European Centre for Medium-Range Weather Forecasts Reanalysis 5; ref. 24) temperature fields at pressure levels, together with the NOAA TLT weighting function (Extended Data Fig. 1; ref. 57), to derive an equivalent TLT. The surface contribution to the TLT is ignored due to uncertainties in surface emissivity. This omission causes the TLT derived solely from the atmospheric weighting function to be slightly smaller than the actual TLT that includes surface contributions. However, we expect the temperature anomaly variations to be similar.

Because MSU, AMSU-A, and ATMS satellite data are assimilated into ERA5(ref. 24), the ERA5 equivalent TLT provides a complementary perspective to satellite-based TLTs. In addition, ERA5 supplies internally consistent forcing fields that influence TLT behavior, thereby serving as a bridge between satellite TLT and the associated forcing fields. For simplicity, we refer to the ERA5-equivalent TLT as the ERA5 TLT throughout the following discussion.

The Extended Data Fig. 2 shows the global monthly mean TLT anomaly time series during 1981-2025 for the NOAA, UAH, RSS, and ERA5.

Removing ENSO and Aerosol Effects in TLT

We use the Niño 3.4 index in this study because it removes ENSO signals from the TLT time series most effectively[29,34]. The Extended Data Fig. 3a shows changes in NINO3.4 from 1981 to 2025, while the Extended Data Fig. 3b shows their lagged correlations with TLT. The strongest correlation occurs when NINO3.4 leads TLT by 5 months. This provides the basis for using the 5-month-lagged NINO3.4 index to remove ENSO effects from the TLT record. The Extended Data Fig. 2 shows the effect of removing the ENSO signal from different TLT datasets using the 5-month-lagged Niño 3.4 index. The jumps associated with the 1998, 2016, and 2023 El Niño events in the original TLT are effectively removed in all datasets.

Scattering and reflection of shortwave solar radiation by sulfate aerosol particles increase planetary albedo, producing a cooling effect on the climate system[30-31]. This effect is evident in the ENSO-adjusted TLT time series (Extended Data Fig.2), which shows a pronounced cooling in mid-1992 following the June 1991 eruption of Mount Pinatubo. To account for aerosol effects, we use aerosol optical depth (AOD) from the MERRA-2 reanalysis (ref. 35). MERRA-2 assimilates bias-corrected AOD observations from the Advanced Very High-Resolution Radiometer (AVHRR), the Moderate Resolution Imaging Spectroradiometer (MODIS) on the Terra and Aqua satellites, the Multi-angle Imaging SpectroRadiometer (MISR) over desert regions, and the ground-based Aerosol Robotic Network (AERONET) measurements. MERRA2 AOD includes contributions from both tropospheric and stratospheric aerosols.

The Extended Data Fig. 3c shows the monthly global-mean MERRA-2 AOD time series and, for comparison, includes MODIS AOD[58-59]. After applying a constant bias correction over the overlapping period, MODIS AOD agrees closely with MERRA-2 AOD, indicating effective assimilation of MODIS observations in MERRA-2.

Volcanic eruptions have a lagged effect on TLT. The length of this delay depends on the method used to estimate lagged correlations between AOD and TLT. We apply a multi-lag regression approach to jointly determine the AOD and ENSO lags, which yields the most effective removal of aerosol effects. The Extended Data Fig. 4 shows two-dimensional lagged correlations between AOD and TLT, and between ENSO and TLT, for all datasets. The ENSO–TLT lag remains 5 months, while the AOD–TLT lag is 8 months across all TLT datasets. This result provides the basis for using an 8-month-lagged AOD to remove aerosol effects from the TLT time series.

The ENSO and aerosol effects are removed using simultaneous regressions of lagged ENSO and AOD against the TLT time series. The resulting datasets are referred to as **ENSO–aerosol-adjusted TLT** datasets and are shown in Extended Data Fig. 2. With El Niño and aerosol effects removed, the adjusted monthly TLT variability is dominated by random noise. To focus on the climate signal, we therefore use annual-mean TLT time series in the subsequent analysis. The global annual-mean anomalies of the adjusted TLT time series are shown in Figures 2, alongside the original annual-mean TLT series in Figure 3 for comparison.

The standard deviations of the detrended original annual-mean TLT anomalies are 0.141, 0.148, 0.144, and 0.138 °C for the NOAA, UAH, RSS, and ERA5 datasets, respectively (Figure 3). Here, the optimal cubic fit is used as the baseline curve for detrending. After removal of ENSO and aerosol effects, the remaining time series exhibits 3–4-year variability. The standard deviations of this residual variability are 0.061, 0.075, 0.077, and 0.069 °C for the NOAA, UAH, RSS, and ERA5 datasets, respectively. Compared with the unadjusted TLT, this represents a reduction in variability of 0.067–0.080 °C, or 46–56%. By substantially reducing short-term variability, the ENSO- and aerosol-adjusted TLT time series allow more robust identification of long-term trends and acceleration. The inferred acceleration and other characteristics of the adjusted TLT datasets are discussed in the main text.

Piecewise linear fitting model

In all the following TLT model-fitting sections, we use data only from 1981 to 2024, reserving 2025 as the model test year in the main text.

The piecewise linear fitting model has been used to investigate trend changes in surface temperature time series[7,36]. In this method, the entire temperature time series is first divided into two periods, with the changepoint denoted as **B**. Linear trend lines, denoted as *y(t)*, are then fitted separately for the first and second periods as follows:

$$y(t) = \begin{cases} a_0 + a_2 t & t \le B \\ (a_0 + a_1) + (a_2 + a_3)t & t > B \end{cases} + e(t)\,, \qquad (1)$$

where t is time, a_0 is the intercept of the first trend line, and a_2 is its slope (trend). The coefficient a_1 represents the level shift of the second trend line, while a_3 captures the difference in trend between the second and first periods. The term $e(t)$ represents the residual of the fitting.

The two trend lines in Equation 1 are generally discontinuous at the changepoint[60], which is physically implausible. To ensure physical consistency, continuity is enforced at the changepoint **B**, resulting in the following constraint:

$$a_1 = -a_3 B. \qquad (2)$$

With this constraint, only three regression coefficients in Equation 1 remain independent. These coefficients are determined by solving an optimization problem.

To identify the timing of a significant trend change, the breakpoint is allowed to vary from 1986 to 2020 across all the datasets and for both the original and ENSO–aerosol-adjusted time series. Extended Data Fig. 5 shows how the RMSE and p-values of the fitting model vary as functions of the changepoint . The vertical dashed lines mark the RMSE minima, which are selected as the optimal changepoints for the piecewise linear model. The RMSE minima are 0.146, 0.148, 0.143, and 0.137 K for the original TLT datasets of NOAA, UAH, RSS, and ERA5, and 0.069, 0.074, 0.073, and 0.071 K for their ENSO–aerosol-adjusted counterparts. These values are very close to those from the optimal cubic fits shown in Figures 2 and 3, indicating that the piecewise linear fits perform comparably to the cubic fits. The p-values are smaller than 0.05, indicating that the fits are statistically significant at most optimal changepoints except for the original RSS and UAH TLT.

Figures 2 and 3 show the piecewise linear fitting model corresponding to the identified changepoints. For the original TLT time series, the changepoints are 2013, 2013, 2013, and 2012 for the NOAA, UAH, RSS, and ERA5 datasets, respectively. For the ENSO-aerosol-adjusted time series, these changepoints shift to 2015, 2015, 2015, and 2014. The trend increases from the first to the second period are about 3–4 times larger for the NOAA, UAH, and ERA5 datasets, but only 1–2 times larger for the RSS TLT. These

differences are closely related to the calibration procedures and satellite-bias adjustments applied to the different satellite records, as discussed in the main text.

Optimal polynomial fitting and its statistical significance

A polynomial regression model of degree *n* for the *TLT* time series takes the form:

$$\Delta TLT(t) = b_0 + b_1 \cdot t + b_2 \cdot t^2 + b_3 \cdot t^3 \ldots + b_n \cdot t^n, \quad (3)$$

where $\Delta TLT(t)$ represents the *TLT* anomaly, *t* is time, and b_i (i = 0, 1, 2, ..., n) are the polynomial coefficients, with b_n being the leading coefficient. The degree *n* is not a predetermined parameter and must be carefully chosen. It should be large enough to capture important nonlinear behavior in the time series but small enough to avoid overfitting. One method for selecting an appropriate polynomial degree is to test the statistical significance of the leading coefficient b_n (ref. 61-62). If the leading coefficient is statistically significant, it indicates that the highest-degree term contributes meaningfully to the model's fit and captures important nonlinear structure. If it is not significant, this may suggest overfitting, and a lower-degree polynomial may be more suitable.

Extended Data Fig. 6 shows polynomial fits up to 5th order for the NOAA, UAH, RSS, and ERA5 datasets. Note that the fits use only data from 1981 to 2024, reserving the 2025 data as a test of the final fitting model used for prediction in the main text. For NOAA and UAH, the 4th- and 5th-order curves closely resemble the 3rd-order fits, which exhibit a wave-like pattern with a clear inflection point around the year 2000. ERA5 behaves similarly, except that the inflection point occurs around 1997. This behavior differs markedly from the linear and quadratic fits, which lack an inflection point. The root mean square error (RMSE) of the fits also decreases from the linear model and levels off starting with the 3rd-order fit (Extended Data Fig. 7). Together, these results indicate that the 3rd- or higher-order polynomials are the most appropriate models for the NOAA, UAH, and ERA5 datasets. In contrast, the 3rd- to 5th-order fits for the RSS dataset closely resemble the quadratic fit and show no discernible tilt near 2000, suggesting that a linear or quadratic model is more suitable for the RSS data.

Each coefficient in model (3), including the leading term, has an associated standard error. A t-test is used to evaluate the null hypothesis that the coefficient equals zero (i.e., it has no effect). This yields a p-value, where a small p-value (< 0.05) indicates that the coefficient is statistically significant. The test is applied to all datasets for both the original and ENSO-aerosol-adjusted time series, and the results are presented in Extended Data Fig. 7.

For the NOAA and ERA5 datasets, the leading coefficients are statistically significant for polynomial fits from linear through cubic order in both the original and ENSO–aerosol-adjusted series. However, when the polynomial degree exceeds three, the leading coefficients become statistically insignificant. Taken together with the changes in curve shape and RMSE behavior from linear to fifth order, these results

indicate that the cubic polynomial is the only appropriate—or optimal—model for the NOAA and ERA5 datasets.

For the UAH and RSS datasets, the leading coefficients are statistically significant only for the linear fit in the original time series, but become significant up to the fourth-order fit in the ENSO–aerosol-adjusted time series. To maintain consistency with the NOAA and ERA5 datasets and to avoid potential overfitting, we select the cubic polynomial as the fitting model for the ENSO–aerosol-adjusted UAH and RSS time series.

In summary, only the linear model is statistically justified for the original UAH and RSS datasets, whereas cubic fits are statistically significant for all ENSO–aerosol-adjusted TLT time series. This is similar to the piecewise fitting results, for which the original NOAA and ERA5 datasets show statistically significant fits, while UAH and RSS do not. In contrast, all ENSO–aerosol-adjusted TLT time series are statistically significant.

Figures 2 and 3 compares the piecewise and cubic fits and their residuals for the original and adjusted TLT in the main text. Figure 4 shows acceleration rates corresponding to the cubic fits to the original and adjusted TLT. Discussion of these results is provided in the main text.

Finally, it is noteworthy that the cubic fit is nearly identical to the locally weighted regression (LOESS, ref. 37) smooth (Extended Data Fig. 8). This agreement is particularly strong for the NOAA and ERA5 TLT time series, for both the original and ENSO–aerosol-adjusted data. LOESS is a robust fitting method capable of capturing complex nonlinear and multimodal relationships in time series[37-38]. In other words, the optimal fit for the NOAA and ERA5 datasets corresponds to a LOESS smooth that can be expressed explicitly as a cubic polynomial. This is an important feature of the cubic fit: it is not only statistically optimal but also provides an explicit functional form that enables climate projections, as discussed in the main text.

Potential driving forces of TLT acceleration

Since effects of ENSO and aerosols on TLT variability have been removed, here, we begin examining other possible drivers behind the accelerated warming trends in the adjusted TLT. The human-induced increases in well-mixed atmospheric greenhouse gases—including carbon dioxide (CO_2), methane (CH_4), and nitrous oxide (N_2O)—impose longwave radiative forcing and are the primary drivers of long-term increases in lower-tropospheric and surface temperatures[41-42]. The observed increase in CO_2 and N_2O follows well-defined quadrative curves (Extended Data Fig. 9). Meanwhile, the increase in CH_4 from 1983 to the present is characterized by a well-defined cubic curve superimposed on a seasonal cycle (Extended Data Fig. 9).

To understand how changes in these greenhouse gases affect TLT behavior, we use the simplified expressions provided by ref. 63 to calculate radiative forcing from CO_2, CH_4, and N_2O concentrations, respectively. The formulations in ref. 63 are derived from line-by-line radiative transfer models and

incorporate shortwave absorption by CH_4 as well as the effects of CO_2–N_2O spectral overlap. As shown in Extended Data Fig. 9d, radiative forcings from CH_4 and N_2O are much smaller than that from CO_2. As a result, although CH_4 concentrations exhibit a cubic trend, their radiative forcing does not display a corresponding cubic behavior capable of driving the observed TLT changes when combined with the dominant CO_2 forcing.

Figures

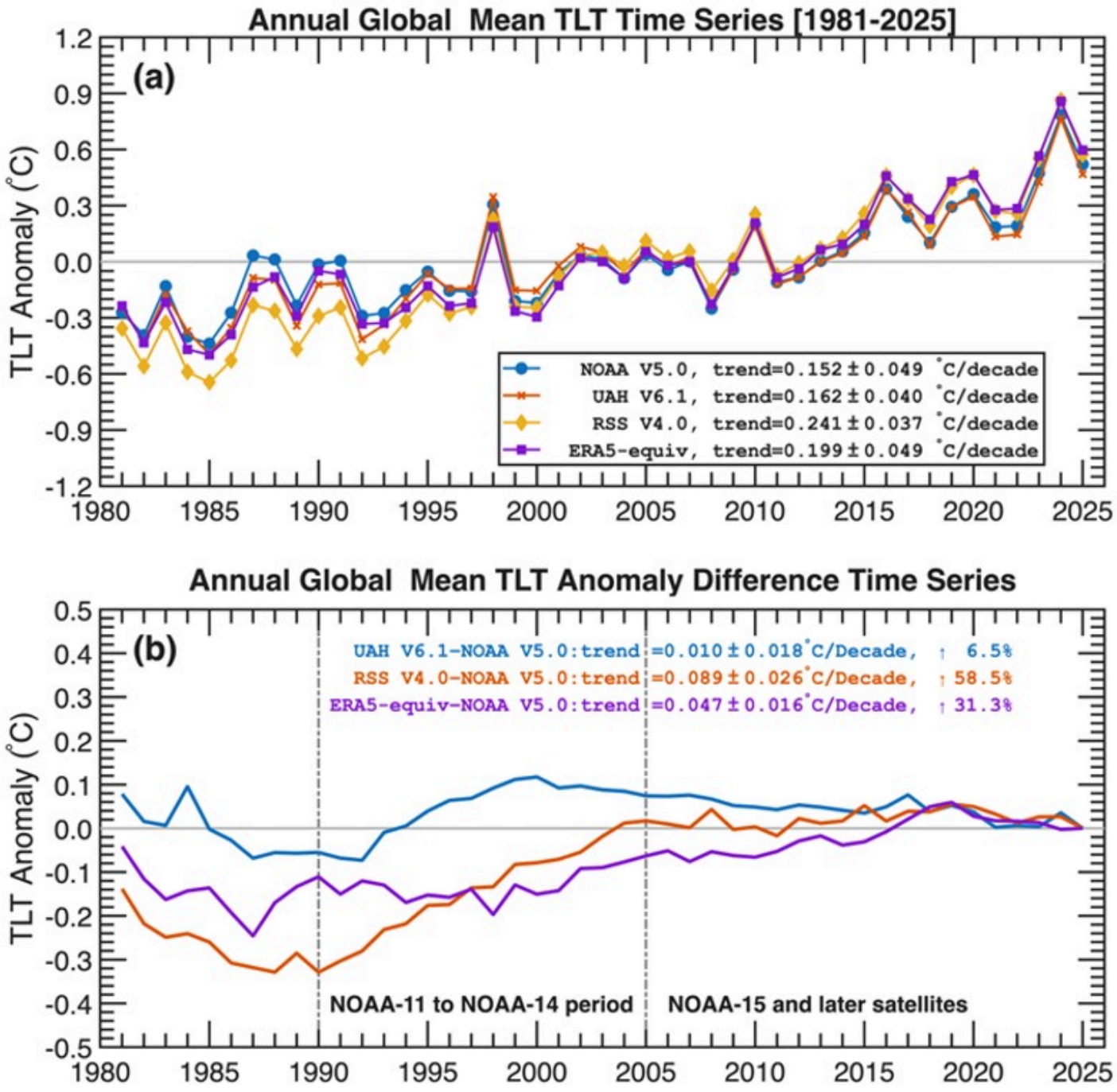

Figure 1

(a) Global annual mean TLT anomaly time series and linear trends during 1981–2025 for the NOAA, UAH, RSS, and ERA5 datasets; (b) Difference time series for these datasets relative to NOAA TLT. The time series are adjusted so that their mean differences in 2025 are set to zero. Vertical lines indicate the start of NOAA-11 around 1990 and the end of NOAA-14 around 2005.

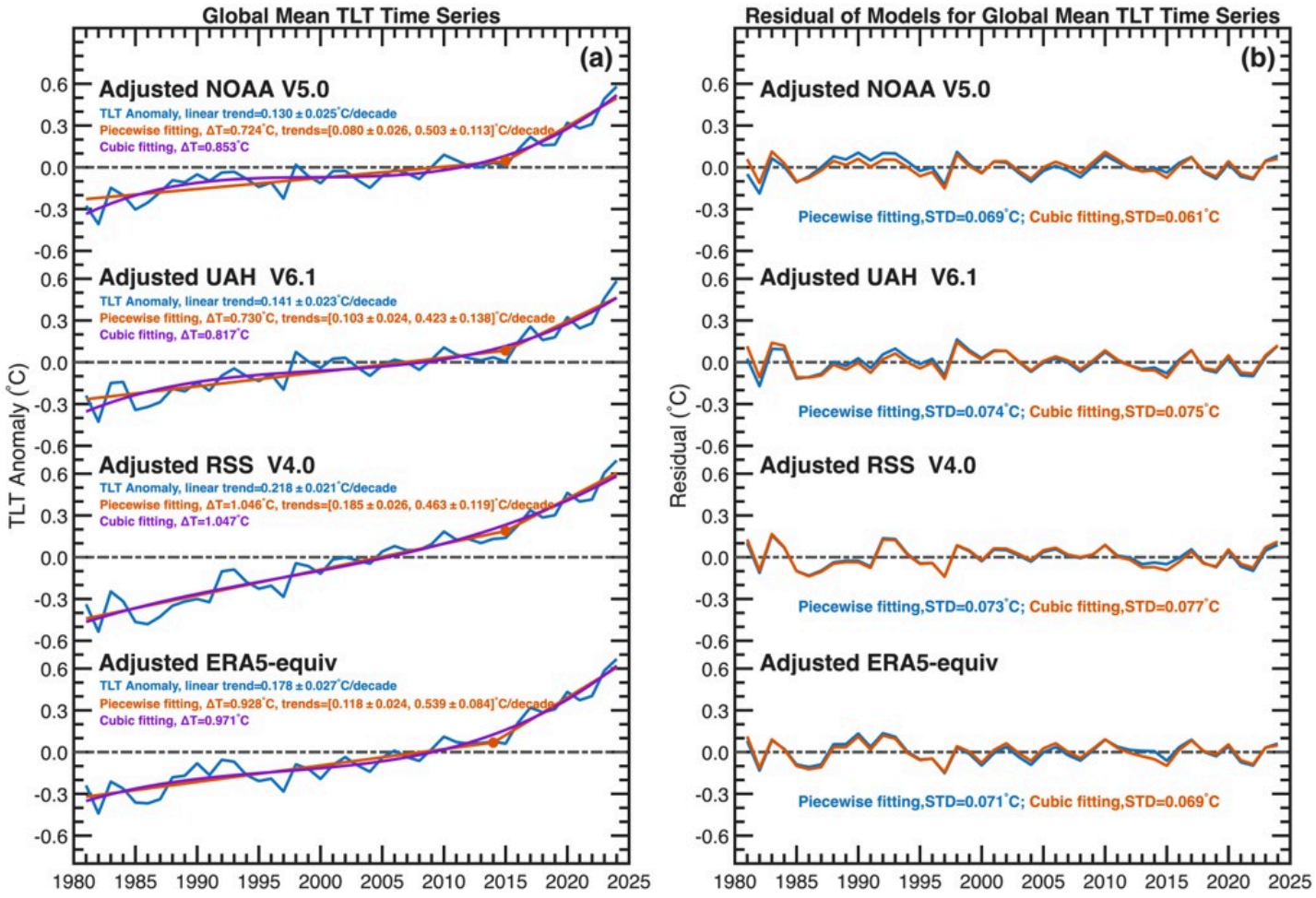

Figure 2

(a) Global annual-mean ENSO–aerosol-adjusted TLT anomalies during 1981–2024 for all datasets, along with their cubic and piecewise fits. (b) Residuals from the fitting models. ΔT in the legend represents the range of the time series (maximum in 2024 minus minimum in 1981) for each fitting model. The red dots in the piecewise model represent the changepoints, and the trend values in square brackets represent those for the first and second periods separated by the changepoints. The trends of the residual time series are zero for both fitting models and across all datasets.

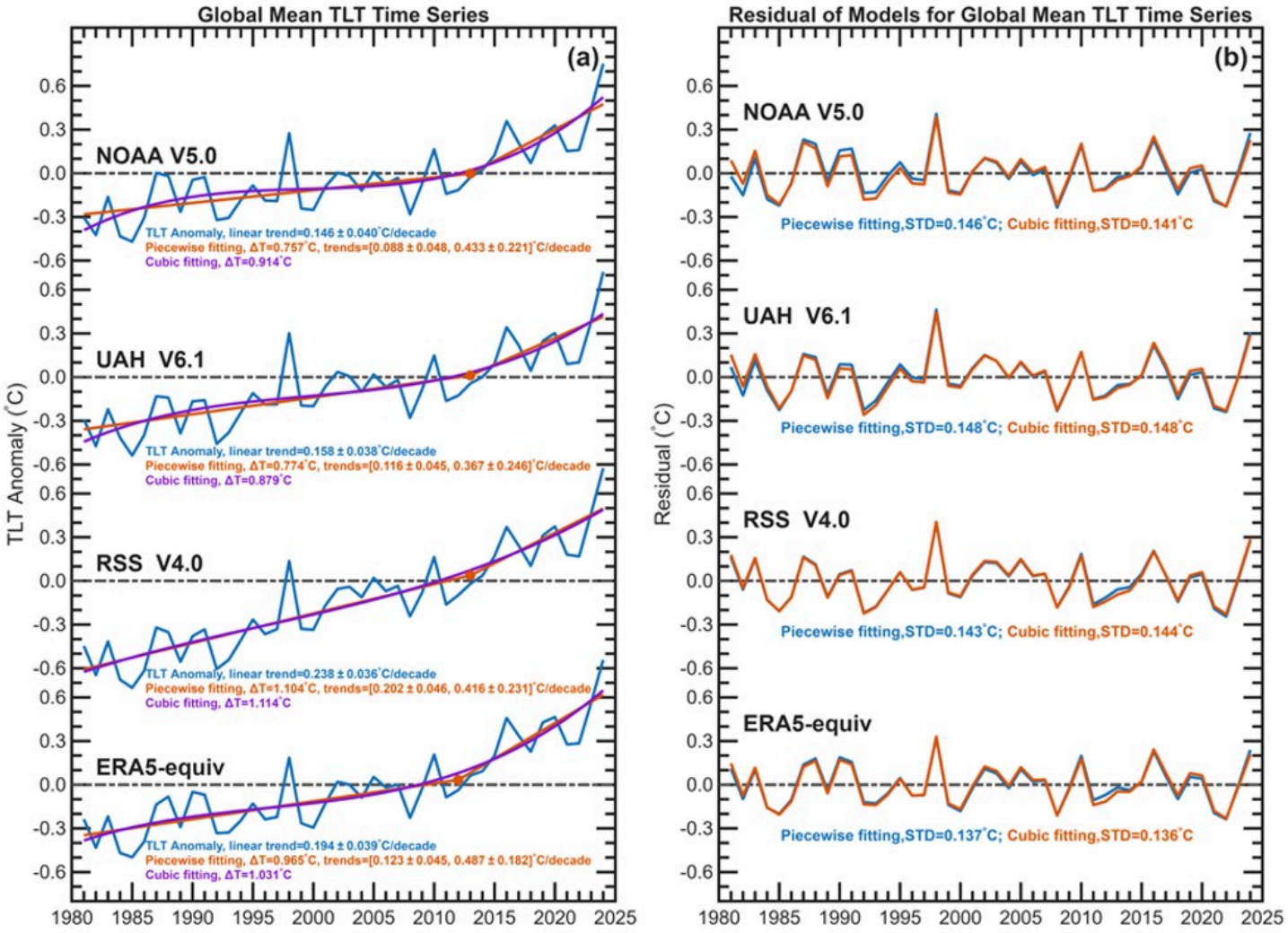

Figure 3

Same as Fig. 2, but for the original TLT.

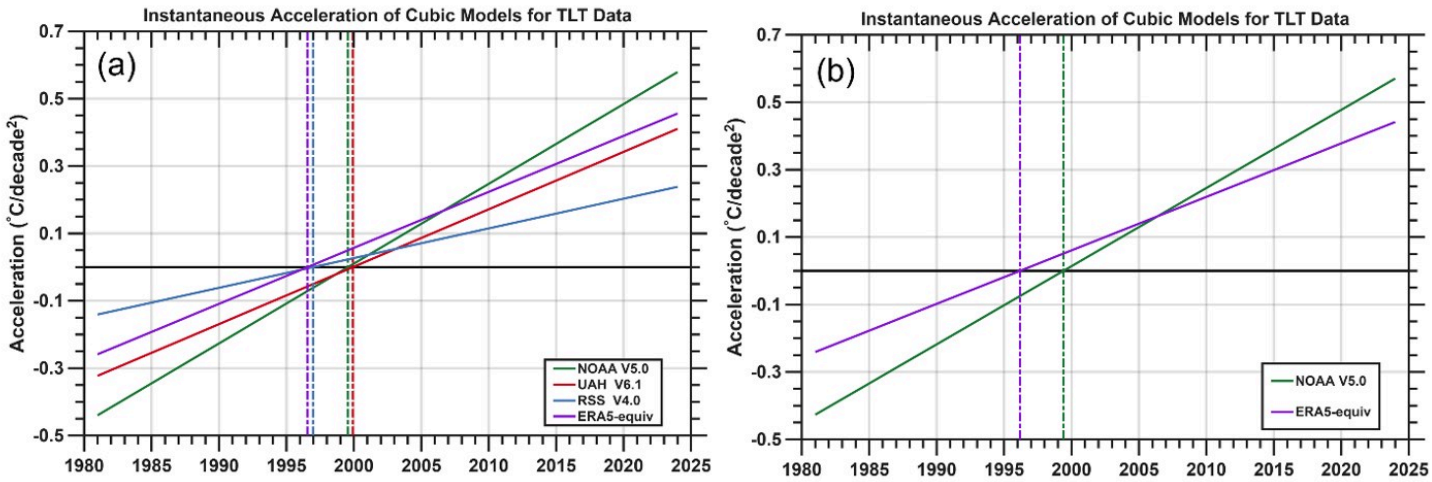

Figure 4

Temporal variation in acceleration rates derived from cubic fits. Vertical lines indicate when the acceleration rate crosses zero for each dataset. (a) ENSO–aerosol-adjusted TLT; (b) original TLT. Only NOAA and ERA5 are shown in (b), as these are the only datasets with statistically significant cubic fits.

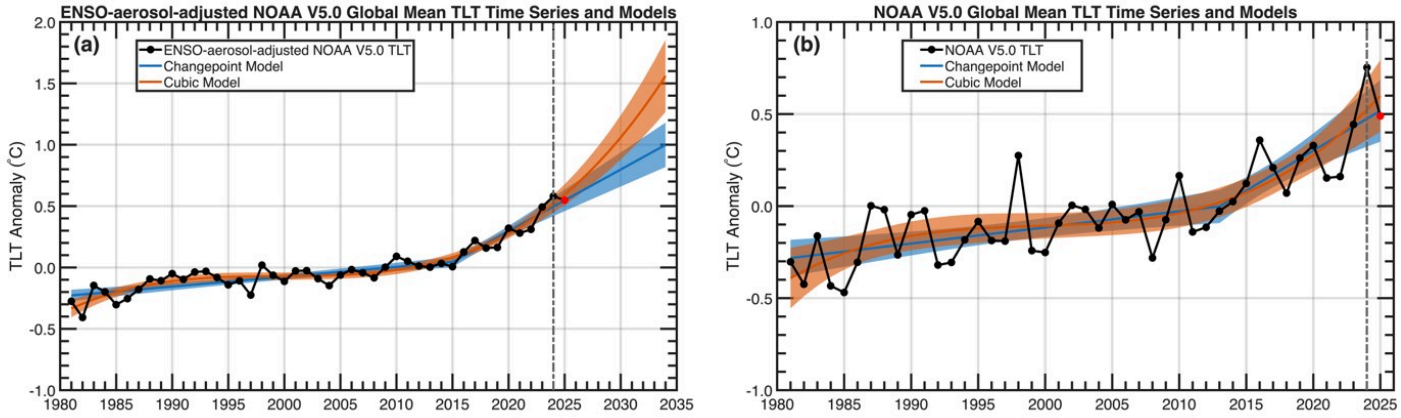

Figure 5

(a) Climate change projections extending up to 2034 for the ENSO–aerosol-adjusted TLT, based on the piecewise (green lines) and cubic (orange lines) fitting models. (b) Same as (a), but for the original NOAA TLT dataset, with projections extending only to 2025. Shaded areas indicate the 95% confidence intervals for the respective models. The red dots at 2025 denote the observed values used to test the one-year projections.

Supplementary Files

This is a list of supplementary files associated with this preprint. Click to download.

- ExtendedData.docx